

Crystallisation of syndiotactic poly(propene-co-octene)

Ralf Thomann, Jörg Kressler* and R. Mülhaupt

Institut für Makromolekulare Chemie und Freiburger Materialforschungszentrum der Albert-Ludwigs-Universität, Stefan-Meier-Str. 21, D-79104 Freiburg i. Br., Germany
(Received 2 September 1996; revised 18 November 1996)

The crystallisation behaviour of syndiotactic poly(propene-co-octene) (P-co-O)-X with octene contents, X , of 4, 15, 20, 40, and 67 wt% is studied by light microscopy, atomic force microscopy (AFM), small angle X-ray scattering (SAXS), wide angle X-ray scattering (WAXS) and differential scanning calorimetry (d.s.c.). The decrease of equilibrium melting points with increasing octene content is in agreement with theoretical values obtained from the copolymer melting equation of Flory. WAXS measurements show that (P-co-O)-4 forms at relatively low supercoolings the type III unit cell known from s-PP homopolymer. For higher supercoolings and for higher octene contents WAXS traces typical for the type II unit cell are observed exclusively. AFM and light microscopical investigations show that the crystalline morphology depends strongly on the octene content. Similar to s-PP homopolymer, (P-co-O)-4 isothermally crystallised at $T_c = 132^\circ\text{C}$ forms single-crystal-like entities and bundle-like morphologies. An important difference to s-PP homopolymer is the absence of cracks and ripples in the single-crystal-like entities, that are typical for s-PP homopolymer. In contrast to s-PP, (P-co-O)-15 forms spherulites at higher crystallisation temperatures and a granular morphology at lower crystallisation temperatures. A similar granular morphology in the nanometer range is also found for (P-co-O)-40. SAXS measurements show that (P-co-O)-15 isothermally crystallised at 90°C forms lamellae with a thickness of approximately 3.5 nm. In the SAXS trace of (P-co-O)-40 a long period cannot be observed. The large scattering at small scattering vectors can be related to the granular morphology. © 1998 Elsevier Science Ltd. All rights reserved.

(Keywords: syndiotactic poly(propene); copolymer; crystallisation)

INTRODUCTION

With the development of single side metallocene catalysts highly syndiotactic poly(propene) (s-PP) has become accessible¹ and the polymorphism of this material has received great attention over the last few years. Two different chain conformations were reported; a planar zigzag form²⁻⁴, and a stable helical conformation with $(\text{TTGG})_2/\text{s}(2/1)2$ symmetry^{5,6}. For the helical conformation three orthorhombic packing models were described⁵⁻⁹; a C-centred cell I with the space group $\text{C}22\bar{2}_1$, a primitive cell II with antichiral packing of chains along the a -axis (space group $\text{P}ca$) and finally a body centred cell III with fully antichiral packing of the chains (space group $\text{I}b\bar{c}a$). The morphology of highly stereoregular s-PP has been reported in some recent publications¹⁰⁻¹³.

The influence of copolymerisation on the crystallisation behaviour of isotactic poly(propene) (i-PP) has been reported elsewhere¹⁴⁻¹⁹. For isotactic poly(propene-co-octene) a decrease of the degree of crystallinity, a decrease of the melting point and an increase of the γ -modification was found with increasing octene contents in the copolymer. The synthesis of syndiotactic poly(propene-co-octene) (P-co-O) and its blend behaviour with atactic poly(propene) was reported by Jüngling *et al.*²⁰ The aim of this paper is to study the crystallisation behaviour of (P-co-O) with varying copolymer composition. Therefore, five random copolymers of (P-co-O)-X having octene contents, X , of 4, 15, 20, 40, and 67 wt% were prepared. The crystallisation behaviour is

then studied by light microscopy, atomic force microscopy (AFM), small angle X-ray scattering (SAXS), wide angle X-ray scattering (WAXS), and differential scanning calorimetry (d.s.c.).

EXPERIMENTAL

Materials

Syndiotactic poly(propene) and random copolymers of propene and octene were prepared using the syndiospecific homogeneous metallocene catalyst $\text{Me}_2\text{C}(\text{Cp})(\text{Flu})\text{Zr Cl}_2/\text{MAO}^{20}$. Characteristic data of all polymers are given in Table 1.

Light microscopy

Samples for light microscopy were prepared by melting the precipitated and dried material between two cover glasses. The layer thickness between these glasses was about 50 μm . The samples were held for 10 min at a temperature of 20°C above the melting point and then quenched to crystallisation temperature at a rate of $30^\circ\text{C min}^{-1}$. The micrographs were taken using an Olympus-Vanox AH2 microscope.

Atomic force microscopy (AFM)

AFM experiments were carried out on a Nanoscope III scanning microscope (Digital Instruments) at ambient conditions. The measurements were performed in the contact mode/height mode (CMHM), tapping mode/height mode (TMHM) and tapping mode/amplitude mode (TMAM). The etching of the samples was carried out in

* To whom correspondence should be addressed

Table 1 Characteristic data of s-PP and (P-co-O)-X

Sample	Octene	Octene	M_n	M_w/M_n	T_g	Diads		
	(wt%)	(mol%)	(g mol ⁻¹)		(°C)	PP	P/O	OO
s-PP	0	0	104 000	1.7	2.7	100	0	0
(P-co-O)-4	4	1.7	73 000	2.1	-0.3	96.2	3.8	n.d.
(P-co-O)-15	15	6.4	94 000	1.7	-5.7	89.3	10.7	n.d.
(P-co-O)-20	20	8.5	62 000	1.6	-7.8	86.6	12.8	0.6
(P-co-O)-40	40	20	76 000	1.9	-16.3	65.3	30.7	4
(P-co-O)-67	67	43	50 000	2.3	-8.4			

an etching reagent prepared by dissolving 50 mg potassium permanganate in a mixture of 4 ml sulfuric acid (95–97%) and 10 g orthophosphoric acid. The samples were immersed in the freshly prepared, green etching reagent at room temperature and held there for 2 h. The etching procedure was supported by an ultrasonic bath. For subsequent washings, sulfuric acid (25%) was cooled near to the freezing point with dry ice and isopropanol. The samples were washed in this acid for ten minutes, in hydrogen peroxide for 5 min and finally in distilled water. Each washing was supported by an ultrasonic bath.

Wide angle X-ray scattering (WAXS)

Samples for WAXS measurements were used as-prepared or isothermally crystallised at various temperatures. The measurements were carried out with a Siemens D500 apparatus. For the measurements the CuK_α radiation of wavelength $\lambda = 0.154$ nm was used.

Small angle X-ray scattering (SAXS)

SAXS measurements were performed in an evacuated Kratky compact camera (Anton Paar K.G.) with an 80 μm entrance slit. Cu K_α radiation with a wavelength of

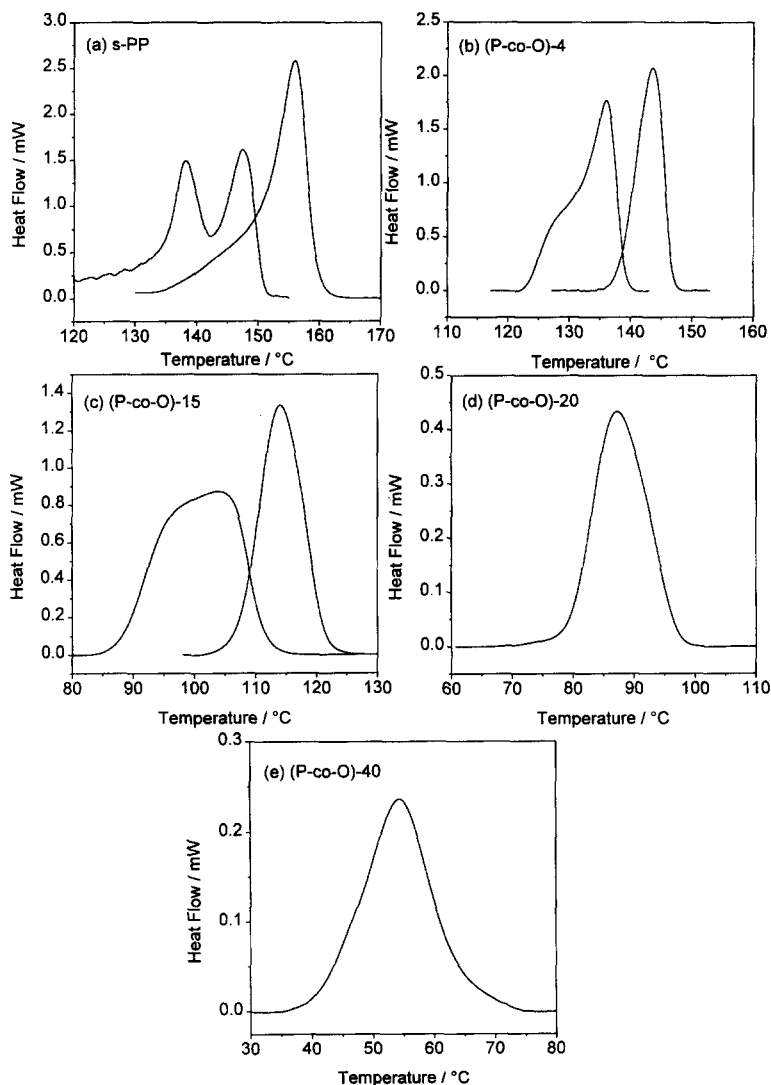


Figure 1 The d.s.c. melting endotherms of isothermally crystallised samples: (a) s-PP homopolymer: $T_c = 90^\circ\text{C}$ (left), $T_c = 115^\circ\text{C}$ (right); (b) (P-co-O)-4: $T_c = 105^\circ\text{C}$ (left), $T_c = 132^\circ\text{C}$ (right); (c) (P-co-O)-15: $T_c = 69.5^\circ\text{C}$ (left), $T_c = 95^\circ\text{C}$ (right); (d) (P-co-O)-20: $T_c = 66^\circ\text{C}$; (e) (P-co-O)-40: T_c = room temperature

$\gamma = 0.154$ nm was used. The scattered intensity, I , was recorded by a scintillation counter in a step-scanning mode at room temperature. The scattering profiles were corrected for background scattering and desmeared. The Fourier transformation of the scattering curve yields the linear correlation function $K(z)$ defined by^{39,40}

$$K(z) = \int_0^\infty 4\pi s^2 I(s) \cos^2 \pi s z ds \quad (1)$$

where s is given by $(2/\gamma) \sin(\Theta/2)$ and Θ is the scattering angle.

Differential scanning calorimetry (d.s.c.)

The d.s.c. measurements were carried out with a Perkin Elmer DSC 7 apparatus. The precipitated or isothermally crystallised samples were heated to 200°C with heating rates of 10, 20 and 30°C min⁻¹. Melting points are obtained by extrapolating the measured values to a heating rate of 0°C min⁻¹.

RESULTS AND DISCUSSION

The d.s.c. measurements

Figure 1a to 1e show d.s.c. melting endotherms of s-PP and of copolymers recorded with a heating rate of 20°C min⁻¹ after isothermal crystallisation. s-PP crystallised at low temperatures, e.g. at 90°C, shows a characteristic dual melting endotherm (Figure 1a left trace). This effect is caused by a melting and recrystallisation process²¹. In the case that the sample is isothermally crystallised at higher temperatures, e.g. at 120°C, a single peak can be observed (Figure 1a right trace). With increasing octene content of the copolymers, the splitting of the endotherm vanishes also for samples crystallised at large supercoolings. For (P-co-O)-4 crystallised at low temperatures the recrystallisation is still visible but less distinguished (left trace of Figure 1b). For (P-co-O)-15 only a broadening of the melting peak can be observed (left trace of Figure 1c). For (P-co-O)-20 and (P-co-O)-40 only single melting endotherms appear at all crystallisation temperatures applied. Obviously, the tremendous decrease of the rate of crystallisation with increasing octene content suppresses the recrystallisation process during the d.s.c. run. For s-PP and for (P-co-O)-4 the single melting endotherm observed after crystallisation at higher temperatures is relatively sharp (right traces in Figure 1a and Figure 1b). The half width at half maximum is about 5°C. With increasing octene content the peaks become broader. For (P-co-O)-40 the half width at half maximum is about 12°C. This broadening is also observed for other olefin copolymers²² and is caused by a broader distribution of the crystallite size with increasing comonomer content.

Figure 2 shows the non-equilibrium melting points, T_m , of s-PP homopolymer and the copolymers after precipitation of the dissolved samples in methanol and drying. Furthermore, the average crystallinity of samples isothermally crystallised from the melt can be seen. All samples for these measurements are crystallised at temperatures where only one melting endotherm can be observed (low supercoolings). In this temperature range, the crystallinity does not depend strongly on the crystallisation temperature. The average crystallinity is calculated by dividing the measured heat of fusion ΔH_m by the theoretical value $\Delta H_{m,100}$ for a 100% crystalline s-PP sample ($\Delta H_{m,100} = 196.6$ J g⁻¹²³). The crystallinity and the melting

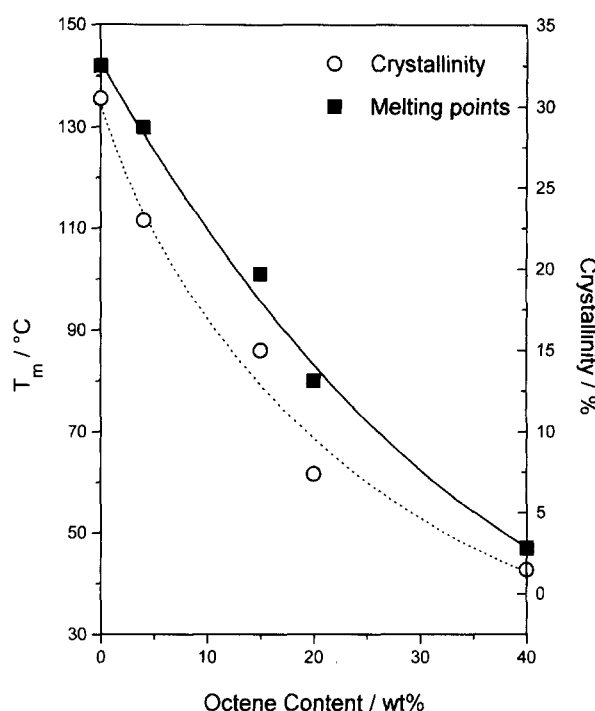


Figure 2 Melting points (squares) of the precipitated samples and average crystallinity (circles) obtained by d.s.c. as a function of copolymer composition

point of the copolymers decrease dramatically with increasing octene content. The copolymer (P-co-O)-67 cannot be crystallised in a reasonable time scale. The decrease of the crystallinity with increasing octene content is caused by the difficulty to reject non-crystallisable octene units in copolymers with higher octene content. Therefore, it might be impossible in the time scale to separate collections of crystallisable sequences of fitting length for crystallisation²².

Equilibrium melting points, T_m , are determined using Hoffman-Weeks plots²⁴. The point of return of the melting endotherm to the baseline is taken as non-equilibrium melting point. This point is taken at three different heating rates for every polymer and extrapolated to a heating rate of 0°C min⁻¹. According to Wunderlich²², the discussion of the melting data of copolymers must be restricted to the highest melting temperature which belongs to the largest and most perfect crystals present (return of the melting endotherm to the baseline of the d.s.c. trace). The equilibrium melting temperatures are obtained from the intersection of the linear extrapolation of T_m as a function of the crystallisation temperature, T_c , with the straight line given by $T_m = T_c$. The experimental data of s-PP and (P-co-O)-4 can only be fitted by straight lines at higher crystallisation temperatures (> 120°C for s-PP and > 110°C for (P-co-O)-4). At lower crystallisation temperatures, where the described recrystallisation process takes place, the melting temperatures are nearly independent of crystallisation temperatures. These points are omitted from the data set. The values of T_m obtained by this method are close to the equilibrium melting point of s-PP homopolymer. Nevertheless, there is a decrease of T_m with increasing octene content (full circles in Figure 3). There have been many efforts to predict the equilibrium melting points of copolymers containing crystallisable and non-crystallisable units²⁵⁻³⁰. The most simple theory assumes that the non-crystallisable component is completely

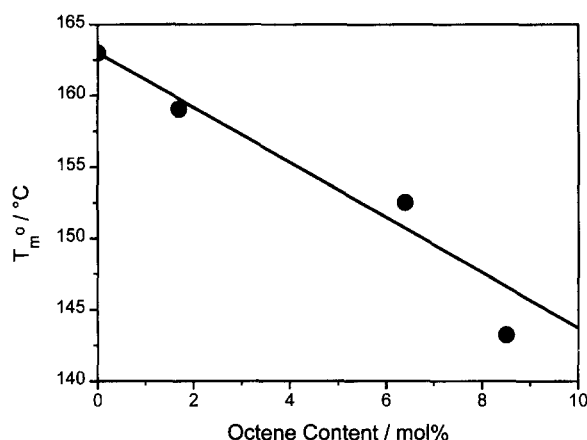


Figure 3 Measured equilibrium melting points (circles), and calculated values (solid line) as a function of copolymer composition

Table 2 Equilibrium melting points calculated by Hoffman-Weeks plots and theoretical values obtained by the copolymer melting equation of Flory²⁵

Sample	T_m ° from Hoffman-Weeks plots (°C)	Theoretical T_m ° (°C)
s-PP	163	—
(P-co-O)-4	159	159.9
(P-co-O)-15	152.5	149.8
(P-co-O)-20	143	146.8
(P-co-O)-40	—	124

excluded from the crystal. For low copolymer contents and large crystallisable homosequences, this theory leads to the copolymer melting equation²⁵

$$(1/T_m \text{ } {}^\circ \text{ copo}) - (1/T_m \text{ } {}^\circ \text{ homo}) = -(R/\Delta h_u) \ln n_A \quad (2)$$

with the equilibrium melting point of the copolymer ($T_m \text{ } {}^\circ \text{ copo}$), the equilibrium melting point of the respective homopolymer ($T_m \text{ } {}^\circ \text{ homo}$), the mole fraction of the

crystallisable component n_A , and the heat of fusion Δh_u . This value is given by the $\Delta H_{m,100}$ value per mole of s-PP repeat units. The assumption of a complete exclusion of the non-crystallisable component from the crystal does not hold for all copolymer systems³⁰⁻³³ but it is valid for the system under investigation as demonstrated below. Therefore, the calculations using equation (2) are in good agreement with our experimental results shown in Figure 3. For the calculation of the equilibrium melting points (full line) using equation (2), $T_m \text{ } {}^\circ \text{ homo} = 536.15 \text{ K}$ and $\Delta h_u = 8257.2 \text{ J mol}^{-1}$ ²³ are taken. Measured and calculated values are also given in Table 2. Taking into consideration the relatively large error of the determination of equilibrium melting points using the Hoffman-Weeks method, the theoretical prediction agrees very well with experimental data.

WAXS measurements

Figure 4 depicts a WAXS trace of (P-co-O)-4 isothermally crystallised at 132°C for 24 days. This WAXS trace is typical for a type III packing mode known from s-PP^{9,34}. Especially the characteristic peak of the type III at $2\Theta = 18.9^\circ$ indexed as 211 is relatively intense. There is a larger amount of type III crystallisation in the copolymer compared with the s-PP homopolymer crystallised at the same supercooling (see ref.⁹). This might be caused by very different rates of crystallisation. The crystallisation rate of the copolymer at that temperature is more than 300 times smaller than the crystallisation rate of s-PP homopolymer at the same supercooling. The inset (a) of Figure 4 depicts the WAXS trace of (P-co-O)-40 isothermally crystallised at room temperature for 2 years. The sample is nearly amorphous. A small crystalline content is indicated by a small shoulder which is in agreement with the small melting endotherm in the d.s.c. trace shown in Figure 1e. The position of the shoulder is similar to the 210/111 peak observed for samples with lower octene content. However, the crystallinity is so small that the packing type (I, II or III) cannot be distinguished. The inset (b) of Figure 4 shows a WAXS trace of as-prepared (P-co-O)-20. The diffraction

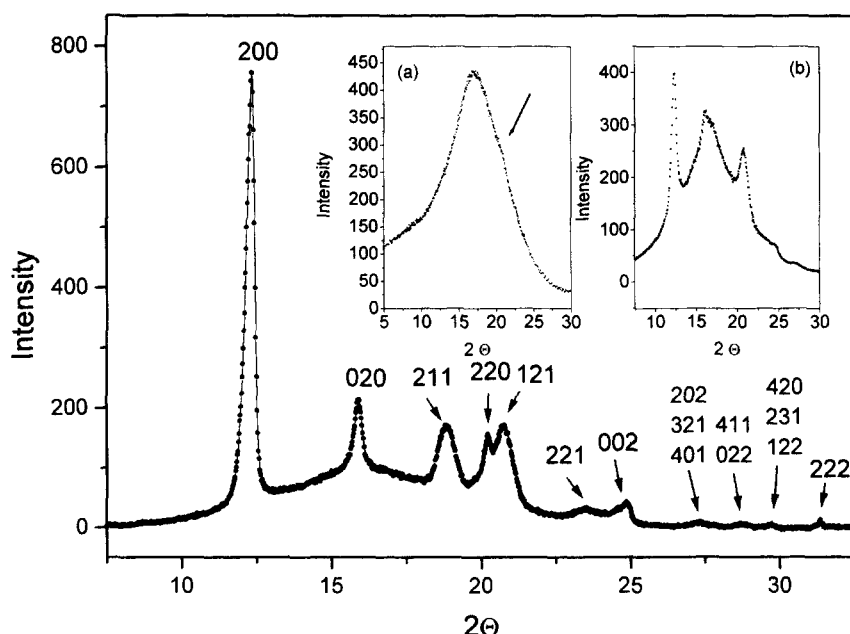


Figure 4 WAXS trace of (P-co-O)-4 isothermally crystallised at 132°C for 24 days. The inset (a) shows the WAXS trace of (P-co-O)-40 crystallised for 2 years at room temperature and inset (b) depicts the WAXS trace of (P-co-O)-20 obtained by precipitation in methanol

pattern is typical for a type II packing mode known from s-PP⁹. The type II packing mode is exclusively observed for all as-prepared copolymers and for (P-co-O)-15 and (P-co-O)-20 isothermally crystallised from the melt. For these samples a type III packing mode could never be observed. There is not any indication for an octene side-chain crystallisation or for a change in the unit cell dimension caused by an incorporation of octene units in the lattice. This supports the assumed exclusion of the octene units from crystalline regions.

Morphology

Morphology of (P-co-O)-4. Figure 5a and Figure 5b shows light micrographs of (P-co-O)-4 isothermally crystallised at 130°C for 22 days and at 132°C for 24 days, respectively. The micrographs show two typical crystalline structures of the copolymer; bundle-like morphologies (Figure 5a) and single-crystal-like entities (Figure 5b). The same morphologies have been reported for s-PP¹³. Similar to s-PP and in contrast to i-PP, this copolymer does not form any spherulites at higher crystallisation temperatures. Cooling the sample rapidly to room temperature leads to small spherulites, visible in the area that surrounds a single crystal-like entity (Figure 6a). The

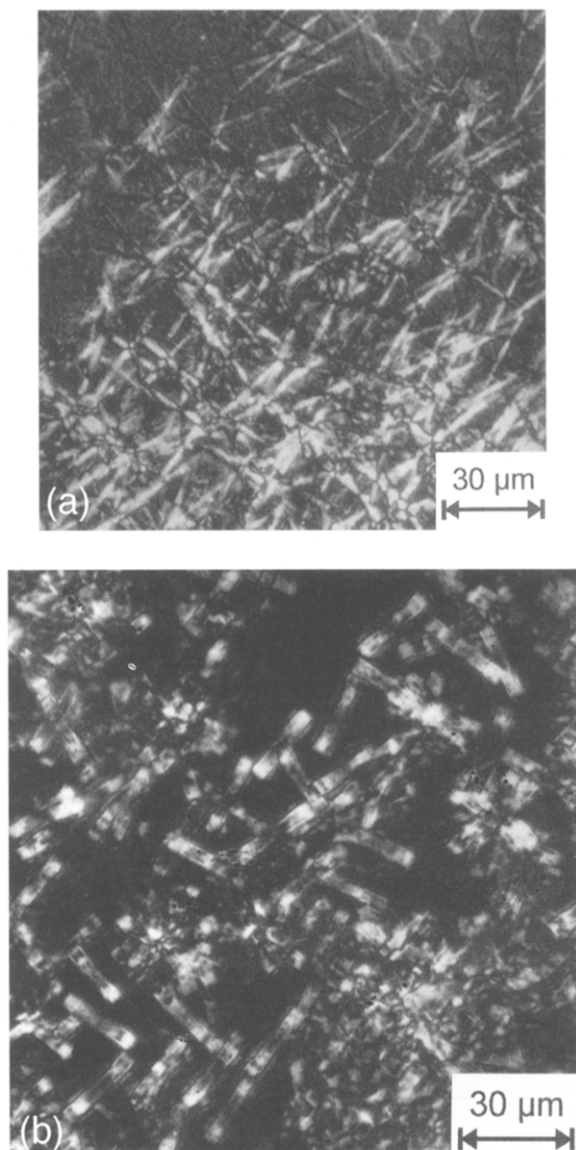
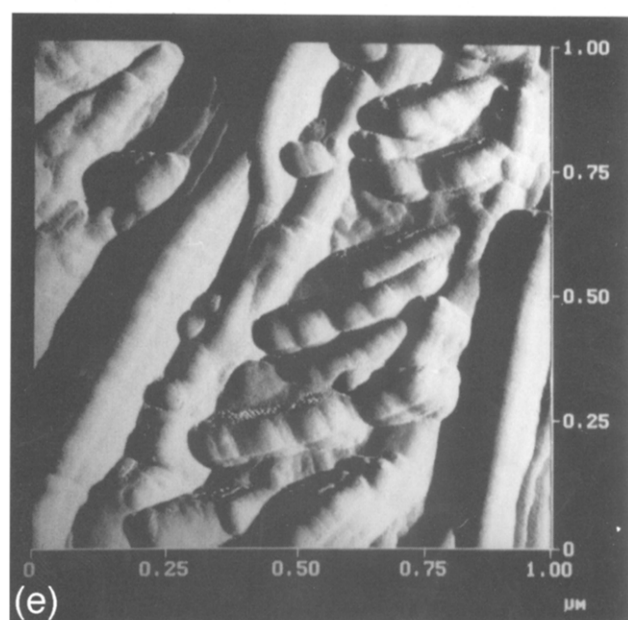
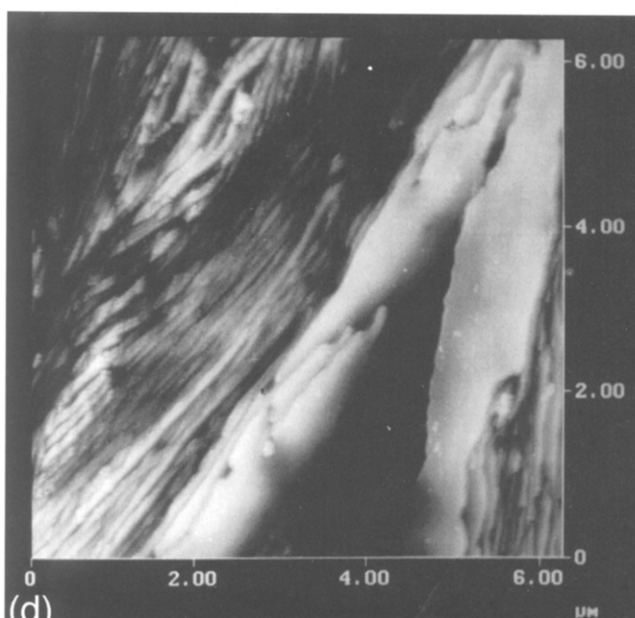
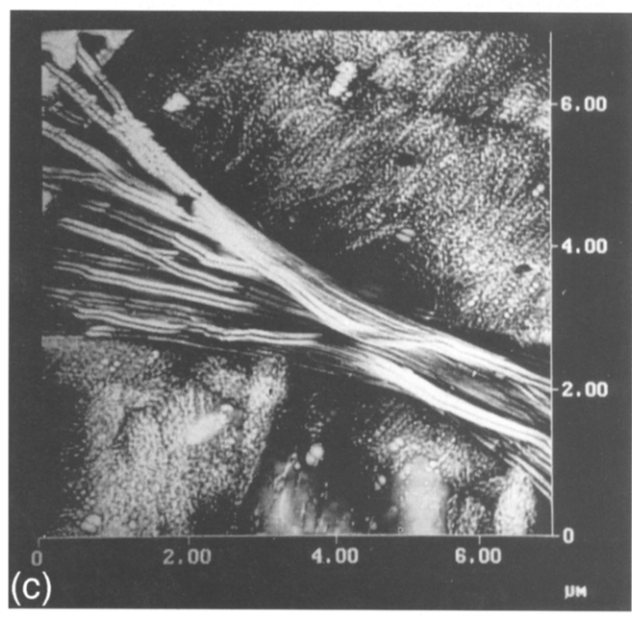
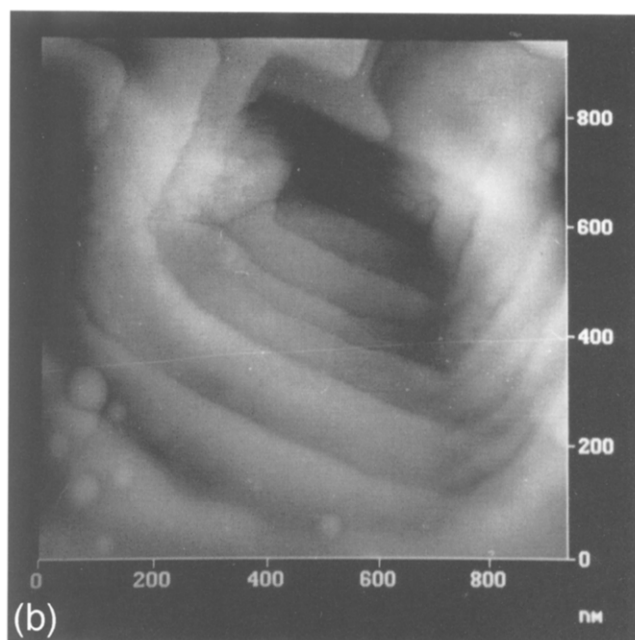
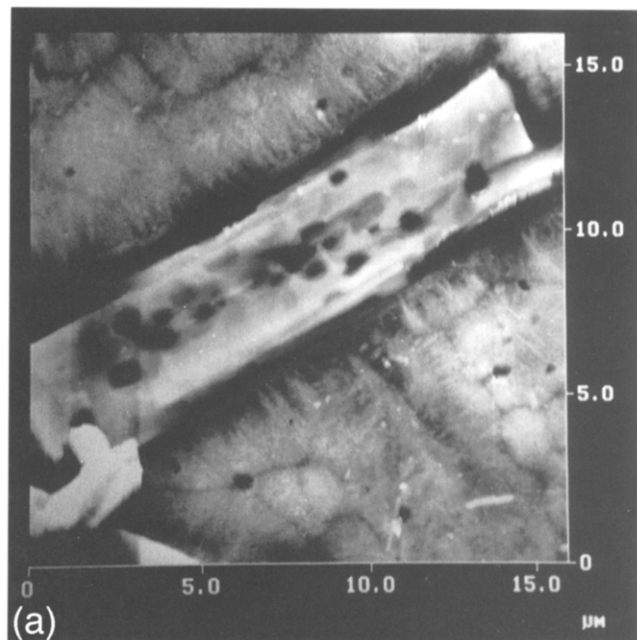


Figure 5 Polarised light micrographs of (P-co-O)-4 isothermally crystallised at: (a) 130°C for 22 days; (b) 132°C for 24 days

impingement lines between spherulites are clearly visible. Furthermore, Figure 6a depicts an AFM micrograph of a single-crystal-like entity formed after crystallisation at 132°C for 24 days. The rectangular shape and the multi-layered architecture of this morphology is similar to s-PP homopolymer, but the quasi-periodic cracks perpendicular to the growth direction which are typical for s-PP homopolymer^{10,13}, are absent. This important difference is a key to a better understanding of the formation of the cracks in s-PP. It has been assumed that the absence of these cracks is caused by a lowering of the mismatch of the thermal expansion coefficients of the crystalline and the chain-fold surface. An explicit description of this mechanism is given elsewhere³⁵. The single-crystal-like entities are disturbed by the formation of large holes. Because the samples for the AFM measurements are etched, it must be discussed, whether these holes could be artifacts or caused by real crystal defects. Usually it is assumed that these etch terraces are formed around actual screw dislocations as discussed for the β -modification of i-PP³⁷. They might be amplified by the etching procedure. The occurrence of real crystal defects is supported by the fact that the etching reagent does not disturb the edges of the rectangular single-crystals which appear very sharp. Furthermore, there are several holes with a rectangular shape. One of them can be seen in Figure 6b. The third important argument is that holes like these are only observed in multilayered single-crystal-like entities, but never in broad lamellae which grow separately and can be observed in samples with a different thermal history (see e.g. Figure 6d). A detailed examination of the defect shown in Figure 6b shows, that the large size must be related to the interconnectivity of the layers in the single-crystal-like entity. These layers are obviously not independently grown. A small defect in one layer initiates growing defects in the layers on top. Figure 6c shows the second typical crystalline morphology of (P-co-O)-4 that appears after isothermal crystallisation at 132°C for 24 days. The bundle-like entities are similar to that observed in s-PP homopolymer¹³. The bundles are formed by separate stacks of lamellae. Figure 6d depicts an AFM micrograph of the same copolymer isothermally crystallised at 110°C for 2 days. The supermolecular structure is formed by broad lamellae. In contrast to the single-crystal-like entities, these lamellae grow independently, and the surface is not disturbed by large holes.

Figure 6e shows an AFM micrograph of (P-co-O)-4 isothermally crystallised at 95°C. The most interesting feature of this sample is the appearance of a morphology that looks similar to the 'cross-hatched' morphology of i-PP³⁶. Short flat-on daughter lamellae grow onto large flat-on mother lamellae (vertical growth direction in the image). The mechanism of the formation of this morphology is different to the 'cross-hatching' process in i-PP samples. The 'cross-hatching' in i-PP is caused by an epitaxial ongrowth of daughter lamellae on mother lamellae in an angle of 80°³⁷. The angle between mother and daughter lamellae in (P-co-O)-4 is about 50°. Furthermore, the 'cross-hatching' in (P-co-O)-4 is only observable in regions with a flat-on orientation of the lamellae. Therefore, it can be assumed, that this ongrowth is caused by a rotational twinning that is also found for single-crystal-like entities of s-PP crystallised at low supercoolings^{10,38}. This type of ongrowth is not observed for s-PP homopolymer when the supercooling is as large as that applied for the crystallisation of (P-co-O)-4. This might be caused by the difference in the



rate of crystallisation of the copolymer and of s-PP homopolymer. At 95°C s-PP homopolymer crystallises relatively fast and does not form well-ordered supermolecular structures. It seems that a slower crystallisation process is necessary for the formation of a 'cross-hatched' morphology by rotational twinning.

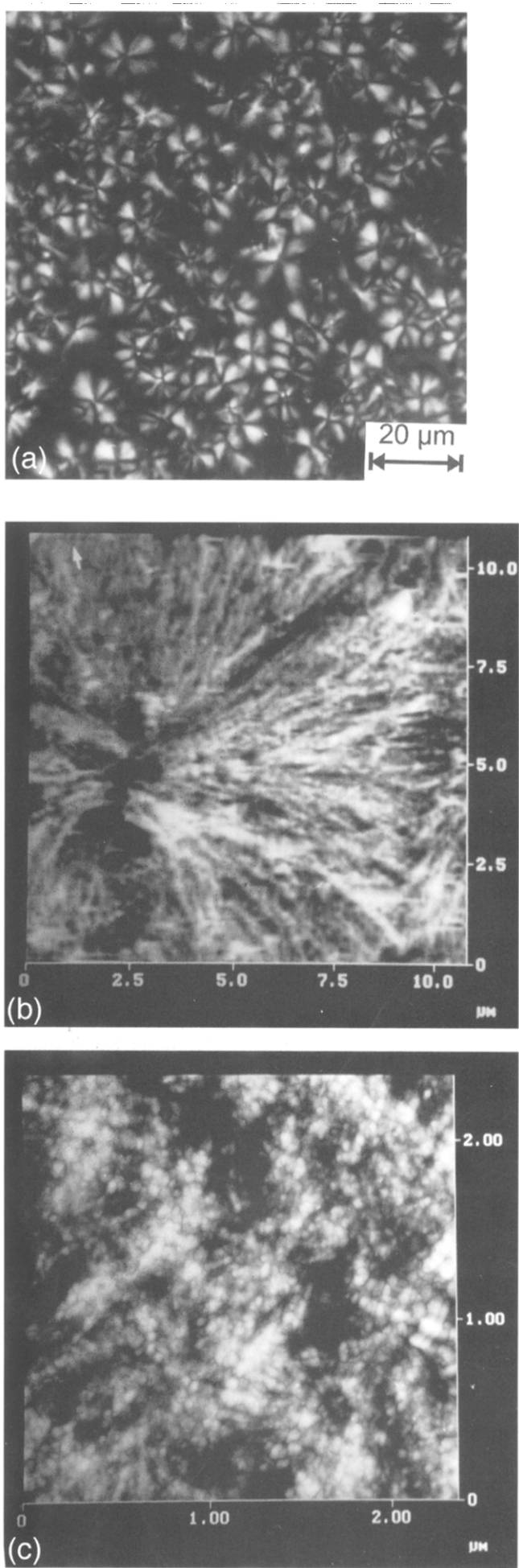
Morphology of (P-co-O)-15. The morphology of (P-co-O)-15 reveals more differences to s-PP homopolymer. Figure 7a shows a light micrograph of a sample isothermally crystallised at 100°C for 21 days. In contrast to the bundle-like entities formed by s-PP homopolymer the copolymer forms spherulites. Figure 7b shows an AFM micrograph of the same sample. The spherulitic morphology is very disordered and contains several small crystalline grains. These grains are the main morphology for copolymers with high octene contents. The change from the bundle-like morphology in s-PP or (P-co-O)-4 to the spherulitic morphology is caused by a more frequent branching of lamellae. This might be caused by an increase of the number of crystal defects with increasing octene content of the copolymers. The grain morphology is even more pronounced when the sample is isothermally crystallised at 65°C (Figure 7c). These grains are relatively disordered and their occurrence is also very characteristic for (P-co-O)-40 as will be discussed below.

The inset of Figure 8 shows the desmeared and corrected SAXS trace for (P-co-O)-15 isothermally crystallised at 90°C. Most characteristic is the maximum which belongs to a long period of about 13 nm. More quantitative information can be deduced from the Fourier transformation of the scattering curve, which yields the linear correlation function, $K(z)$, according to equation (1) (see Figure 8). The lamella thickness obtained from the self-correlation triangle^{39,40} is approximately 3.5 nm.

Morphology of (P-co-O)-40. It has been shown above that (P-co-O)-40 is able to crystallise (thought only in a very large time scale). Figure 9 shows the desmeared SAXS trace of (P-co-O)-40 isothermally crystallised at room temperature for 2 years and for comparison the desmeared SAXS trace of (P-co-O)-15 isothermally crystallised at 90°C. There does not exist any maximum in the SAXS trace for (P-co-O)-40. A very strong scattering at small s -values is most characteristic and much more intense than that in the scattering profile of (P-co-O)-15. The explanation for this behaviour can be obtained from the observation of the morphology by AFM of the same sample after etching. Figure 10 shows the 3D AFM image of (P-co-O)-40 with the same thermal history as the sample used for SAXS. A granular morphology is visible, formed by grains with diameters ranging from 15 to 50 nm. These grains are packed into clusters. This morphology is responsible for the intense scattering at small s -values. Granular structures are also found, e.g. for very low density polyethylene and they are assumed to be formed by fringed micelles⁴¹.

Figure 6 AFM (TMHM) micrographs of (P-co-O)-4 isothermally crystallised at 132°C for 24 days (a–c): (a) multilayered single-crystal-like entity; (b) a hole in the single-crystal-like entity; (c) a bundle-like morphology; (d) broad lamellae crystallised isothermally at 110°C (AFM TMHM); (e) a twinning morphology of (P-co-O)-4 isothermally crystallised at 95°C (AFM TMAM)

Figure 7 (a) Light micrograph of (P-co-O)-15 isothermally crystallised at 100°C; (b) AFM micrograph of the same sample; (c) AFM (TMHM) micrograph of (P-co-O)-15 crystallised at 65°C



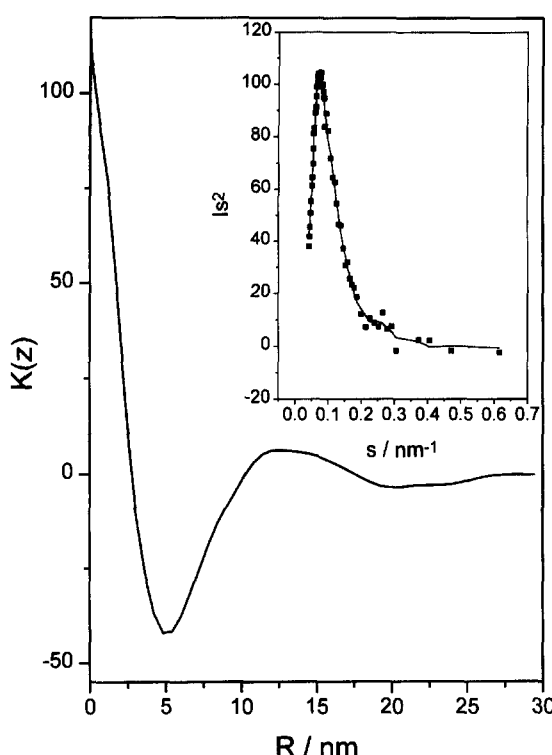


Figure 8 Correlation function $K(z)$ of (P-co-O)-15 crystallised at 90°C. The inset shows the desmeared and corrected SAXS trace

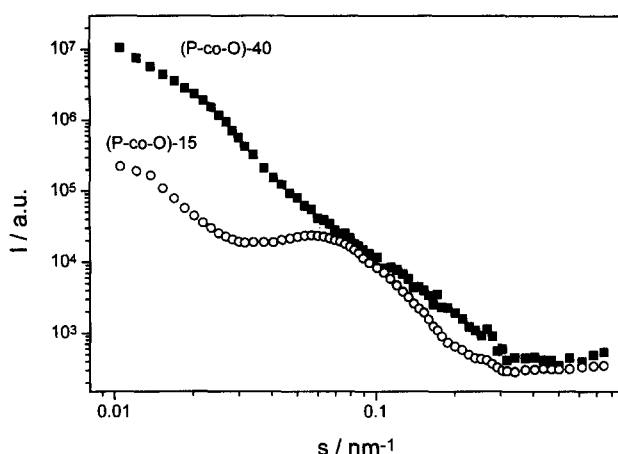


Figure 9 Desmeared SAXS trace of (P-co-O)-40 (squares) crystallised at room temperature for 2 years. For comparison the desmeared SAXS trace of (P-co-O)-15 (circles) is shown

CONCLUSION

Syndiotactic copolymers of propene and octene form a large variety of crystalline morphologies depending on the copolymer composition and supercooling. Copolymers with a small octene content are able to form single-crystal-like entities and bundle-like morphologies similar to s-PP. An important difference to s-PP homopolymer is the absence of cracks and ripples in the single-crystal-like entities. But the single-crystal-like entities are disturbed by the formation of large holes. The size of these holes must be related to the interconnectivity of the layers in the single-crystal-like entity. In contrast to s-PP, (P-co-O)-15 forms spherulites at higher crystallisation temperatures and a granular morphology at lower crystallisation temperatures. A similar granular morphology is also found

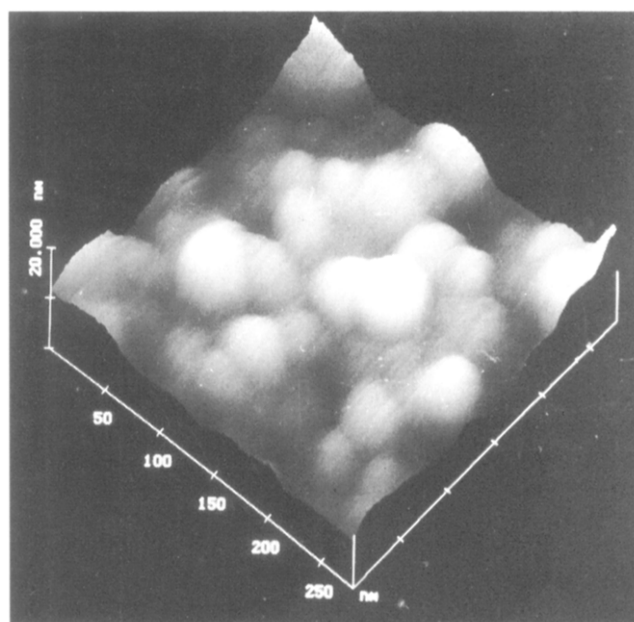


Figure 10 AFM (CMHM) micrograph of (P-co-O)-40 isothermally crystallised for 2 years at room temperature

for (P-co-O)-40. SAXS measurements show, that (P-co-O)-15 isothermally crystallised at 90°C forms lamellae with a thickness of approximately 3.5 nm. In the SAXS trace of (P-co-O)-40 a long period is absent. The SAXS trace shows a large scattering intensity at small scattering vectors that is caused by the granular morphology mentioned. The d.s.c. measurements show a decrease of the melting points and of the crystallinity with increasing octene content. Equilibrium melting points determined from Hoffmann-Weeks plots show only a slight decrease with increasing octene content. This decrease can be predicted from the copolymer melting equation of Flory and indicates an exclusion of octene units from the crystal lattice. WAXS measurements show that (P-co-O)-4 forms at relatively low supercoolings the type III unit cell known from s-PP homopolymer. For higher supercoolings and for higher octene contents, WAXS traces typical for the type II unit cell are obtained.

REFERENCES

1. Ewen, J. A., Jones, R. L., Razavi, A. and Ferrara, J. D., *Journal of the American Chemical Society*, 1988, **110**, 6255.
2. Turner-Jones, A. and Cobbald, A. J., *Journal of Polymer Science (B), Polymer Letters Edition*, 1968, **6**, 539.
3. Natta, G., Peraldo, M. and Allegra, G., *Makromolekulare Chemie*, 1964, **75**, 215.
4. Chatani, Y., Maruyama, H., Noguchi, K., Asanuma, T. and Shimura, T., *Journal of Polymer Science (C), Polymer Letters Edition*, 1990, **28**, 393.
5. Corradini, P., Natta, G., Ganis, P. and Temussi, P. A., *Journal of Polymer Science, Part (C)*, 1967, **16**, 2477.
6. Lotz, B., Lovinger, A. J. and Cais, R. E., *Macromolecules*, 1988, **21**, 2375.
7. Lovinger, A. J., Lotz, B. and Davis, D. D., *Polymer*, 1990, **31**, 2253.
8. Lovinger, A. J., Davis, D. D. and Lotz, B., *Macromolecules*, 1991, **24**, 552.
9. De Rosa, C. and Corradini, P., *Macromolecules*, 1993, **26**, 5711.
10. Lovinger, A. J., Lotz, B., Davis, D. D. and Schumacher, M., *Macromolecules*, 1994, **27**, 6948.
11. Schumacher, M., Lovinger, A. J., Agarwal, P., Wittmann, J. C. and Lotz, B., *Macromolecules*, 1994, **28**, 1370.
12. Tsukruk, V. V. and Reneker, D. H., *Macromolecules*, 1995, **28**, 1370.
13. Thomann, R., Wang, C., Kressler, J., Jüngling, S. and Mühlaupt, R., *Polymer*, 1995, **36**, 3795.

14. Turner Jones, A., *Polymer*, 1971, **12**, 487.
15. Guidetti, G. P., Busi, P., Giulianetti, I. and Zanetti, R., *European Polymer Journal*, 1983, **19**, 757.
16. Busico, V., Corradini, P., De Rosa, C. and Di Benedetto, E., *European Polymer Journal*, 1985, **21**, 239.
17. Avella, M., Martuscelli, E., Della Volpe, G., Segre, A., Rossi, E. and Simonazzi, T., *Makromolekulare Chemie*, 1986, **187**, 1927.
18. Marigo, A., Marega, C., Zanetti, R., Paganetto, E., Canossa, E., Coletta, F. and Gottardi, F., *Makromolekulare Chemie*, 1989, **190**, 2805.
19. Mezghani, K. and Phillips, P. J., *Polymer*, 1995, **35**, 2407.
20. Jüngling, S., Mülhaupt, R., Fischer, D. and Langhauser, F., *Angewandte Makromolekulare Chemie*, 1995, **229**, 93.
21. Rodriguez-Arnold, J., Zhang, A., Cheng, S. Z. D., Lovinger, A. J., Hsieh, E. T., Chu, P., Johnson, T. W., Honell, K. G., Geerts, R. G., Palackal, S. J., Hawley, G. R. and Welch, M. B., *Polymer*, 1994, **35**, 1884.
22. Wunderlich, B., *Macromolecular Physics*, Vol. 1. Academic Press, New York, 1980.
23. Hafka, S. and Könnecke, K. J., *Macromolecular Science*, 1991, **B30**, 319.
24. Hoffman, J. D. and Weeks, J. J., *Journal of Research of the National Bureau of Standards*, 1962, **A33**, 13.
25. Richardson, M. J., Flory, P. J. and Jackson, J. B., *Polymer*, 1963, **4**, 221.
26. Baker, C. H. and Mandelkern, L., *Polymer*, 1966, **7**, 7.
27. Baur, H., *Makromolekulare Chemie*, 1966, **98**, 297.
28. Sanchez, I. C. and Eby, R. K., *Journal of Research of the National Bureau of Standards*, 1973, **77**, 353.
29. Helfand, E. and Lautitzen, J. I. Jr., *Macromolecules*, 1973, **6**, 631.
30. Sanchez, I. C. and Eby, R. K., *Macromolecules*, 1975, **8**, 638.
31. Colson, J. P. and Eby, R. K., *Journal of Applied Physics*, 1966, **37**, 3511.
32. Alfonso, G. C., Fiorina, L., Martuscelli, E., Pedemonte, E. and Russo, S., *Polymer*, 1973, **14**, 373.
33. Parel, G. N. and Keller, A., *Journal of Polymer Science, Polymer Physics Edition*, 1975, **13**, 2281.
34. Lovinger, A. J., Lotz, B., Davis, D. D. and Padden, F. J., *Macromolecules*, 1993, **26**, 3494.
35. Thomann, R., Kressler, J. and Mülhaupt, R., *Macromolecular Chemistry and Physics*, 1997, **198**, 1271.
36. Bassett, D. C. and Olley, R. H., *Polymer*, 1984, **25**, 935.
37. Norton, D. R. and Keller, A., *Polymer*, 1985, **26**, 704.
38. Thomann, R., Kressler, J., Setz, S., Wang, C. and Mülhaupt, R., *Polymer*, 1996, **37**, 2627.
39. Strobl, G. R., Schneider, M. J. and Voigt-Martin, I. G., *Journal of Polymer Science, Polymer Physics Edition*, 1980, **18**, 1361.
40. Tanabe, Y., Strobl, G. R. and Fischer, E. W., *Polymer*, 1986, **27**, 1147.
41. Minick, J., Moet, A., Hiltner, A., Baer, E. and Chum, S. P., *Journal of Applied Polymer Science*, 1995, **58**, 1371.